Numerical study of the initial condition and emission on simulating PM$_{2.5}$ concentrations in Comprehensive Air Quality Model with extensions version 6.1 (CAMx v6.1): Taking Xi'an as example

Han Xiao [1], Qizhong Wu [1*], Xiaochun Yang [1,2], Lanning Wang[1], Huaqiong Cheng[1]

[1] College of Global Change and Earth System Science, Beijing Normal University, Beijing 100875, China
[2] Xi'an Meteorological Bureau, Xi'an, Shaanxi Province 710016, China

Correspondence to: Qizhong Wu (wqizhong@bnu.edu.cn)

Abstract. A series of model sensitivity experiments is designed to explore the effects of different initial conditions and emissions in Xi'an in December 2016, which is a major city in the key area "Fen-Wei Plains" for air pollution control in China. Three methods were applied for the initial condition tests: clean initial simulation, restart simulation and continuous simulation. In clean initial simulation test, the sensitivity experiments C00, C06, C12, C18, and C24 were conducted according to the intercepted time periods, and the results showed that the model performance of PM$_{2.5}$ was better with the delay of the start time of the intercepted time periods. From experiments C00 to C24, the absolute mean bias (MB) decreased from 51.07 μg/m^3 to 3.72 μg/m^3 and the index of agreement (IOA) increased from 0.49 to 0.86, which illustrates that the model performance of C24 is much better than C00. In order to explore the restart simulation, sensitivity experiments R1120 and R1124 were set according to the time of the first day for the model simulation. Although the start times of simulations were different, after a period of spin-up time, the simulation results with different start time were nearly consistent, the results showed that the spin-up time is about 27 hours. As for the continuous simulation test, CT12 and CT24 were conducted. The start time of the intercepted time periods for CT12 and R1120 were the same, and the simulation results were nearly identical. The simulation results of CT24 performed best in all the sensitivity experiments, with the correlation coefficient (R), MB, and IOA reaching 0.81, 6.29 μg/m^3, and 0.90, respectively. For the emission tests, the updated local emission inventory with construction fugitive dust emissions have been added and compared to the simulation results of the original emission inventory. The simulation with the updated local emissions showed a much better performance on PM$_{2.5}$ modelling. Therefore, combining the method of CT24 with the updated local emission inventory can nicely improve the model performance of PM$_{2.5}$ in Xi'an, the absolute MB decreased from 35.16 μg/m^3 to 6.29 μg/m^3 and the IOA reached 0.90.

1 Introduction

In the recent years, severe air pollution has gradually become a big challenge in China and other developing countries (Wu et al., 2014; Li et al., 2017a). China released three-year action plan for cleaner air in 2018, and efforts will be focused on areas including the Beijing-Tianjin-Hebei region, the Yangtze River Delta, and the Fen-Wei Plains. As a major city in the key area "Fen-Wei Plains", Xi'an is located in the Guanzhong Basin. The city is surrounded by the Qinling Mountains to the south, and

the Loess Plateau extends to the north and west, which is not conductive to the spread of air pollutant. Xi'an has suffered serious air pollution in recent years because of its special topography and rapid economic development (Zhang, et al., 2002; Cao, et al., 2012). Worse, Xi'an is under rapid development of urban construction activities with large construction fugitive dust (Long et al., 2016).

35 Air quality modelling systems is an important tool for air pollution assessment and have evolved over three generations since the 1970s, driven by crucial regulations, societal and economic needs, and increasing high performance computing capacity (Zhang et al., 2012). Various air quality models are widely used in the simulation and forecasting of pollutants, such as the Community Multiscale Air Quality (CMAQ) (Eder and Yu, 2006; Appel et al., 2017), the Comprehensive Air Quality Model with extensions (CAMx) (ENVIRON, 2013), WRF-Chem (Grell et al., 2005), and the Nested Air Quality Prediction

40 Modeling System (GNAQPMS/NAQPMS) (Wang et al., 2006; Chen et al., 2015; Wang et al., 2017). In order to accurately analyze the apportionment of emission categories and contributions from different source regions for atmospheric pollutions, many researchers used the CAMx model with the particulate matter source apportionment technology (PSAT) in different areas of China, including Beijing (Zhang et al., 2018), Tangshan (Li et al., 2013), Pearl River Delta region (Wu et al., 2013) and Yangtze River Delta region (Li et al., 2011). The CAMx showed good model performances for simulation of air pollution

45 (Panagiotopoulou et al., 2016).

The input files for CAMx model include initial/boundary conditions, gridded and elevated point source emissions, and meteorological files (ENVIRON, 2013). The meteorology and emissions inputs can cause great uncertainty for air quality models (Tang et al. 2010; Gilliam et al., 2015). Many researchers reduced the uncertainty of meteorology through refined physical parameterizations and other techniques such as data assimilation (Sistla et al., 1996; Seaman, 2000; Gilliam et al.,

50 2015; Li et al., 2019). A reasonable emission inventory is very important for the simulation accuracy of the air quality model. Many researchers studied East Asian emissions (Kato et al., 1992; Streets et al., 2003; Ohara et al. 2007; Zhang et al., 2009;), and tried to construct emission inventories of particulate matter (PM) in China (Wang et al. 2005; Zhang et al. 2006). However, the absence of detailed information on China introduces great uncertainty into the emission inventories (Cao et al., 2011). In recent years, more and more researchers focused on constructing and updating of regional local emission inventories to

55 improve the model performance. Wu et al. (2014) improved the model performance by adding more regional point source emissions and updating the area source emissions in village and surrounding cities of Beijing. Based on that work, Yang et al. (2019) have added local datasets into the emission inventory of Guanzhong Plain, China, which was applied in simulating $PM_{2.5}$ concentrations by CMAQ model in Xi'an. Numerous works indicated that construction dust emission plays an important role of the air pollution, especially in urban areas (Ni et al., 2012; Huang et al., 2014; Wang et al., 2015). In our previous study,

60 we built a particulate matter emission inventory from construction activities at county level in Xi'an, based on an extensive survey of construction activities and combining with two sets of dust emission factors for the typical city in north China (Xiao et al., 2019).

However, few studies have investigated the effects of initial condition on the simulation or prediction of $PM_{2.5}$ concentrations. Therefore, the purpose of this study was to explore the effects of different initial simulation and emissions on

65 the model performance of PM₂.₅ in the CAMx model. A series of model sensitivity experiments for the initial simulation and emissions are designed to find a suitable method for simulating PM$_{2.5}$ concentrations with the reasonable initial condition and emission inventory. Not only for Xi'an, other cities may apply the similar research method using for simulating PM$_{2.5}$ concentrations in the future.

The paper is organized as follows. Section 2 gives the model descriptions for WRF-SMOKE-CAMx model system,
70 including meteorological fields, air quality model descriptions, model domain, emission inventory and processes in Sects 2.1-2.4. Section 3 presents the sensitivity experiments design of different initial condition and emission. Section 4 discuss the model performance of the initial condition tests and emission tests to simulate the PM$_{2.5}$ concentration model in Xi'an. The conclusions are given in Section 5.

2 WRF-SMOKE-CAMx model descriptions

75 In this study, the National Center for Atmospheric Research (NCAR) Weather Research and Forecasting (WRF v3.9.1.1) model (Skamarock et al., 2008), the Center for Environmental Modeling for Policy Development (CEMPD) Sparse Matrix Operator Kernel Emissions (SMOKE v2.4) (Houyoux and Vukovich, 1999) and the Ramboll Environ Comprehensive Air Quality Model with Extensions (CAMx v6.1) (ENVIRON, 2013) were used to build up the air quality model system as shown in Fig.1. The WRF model provided the meteorological conditions for the SMOKE and CAMx model. And the SMOKE model
80 was used to process the emissions data and provide 4-D, model-ready gridded emissions for the air quality model CAMx.
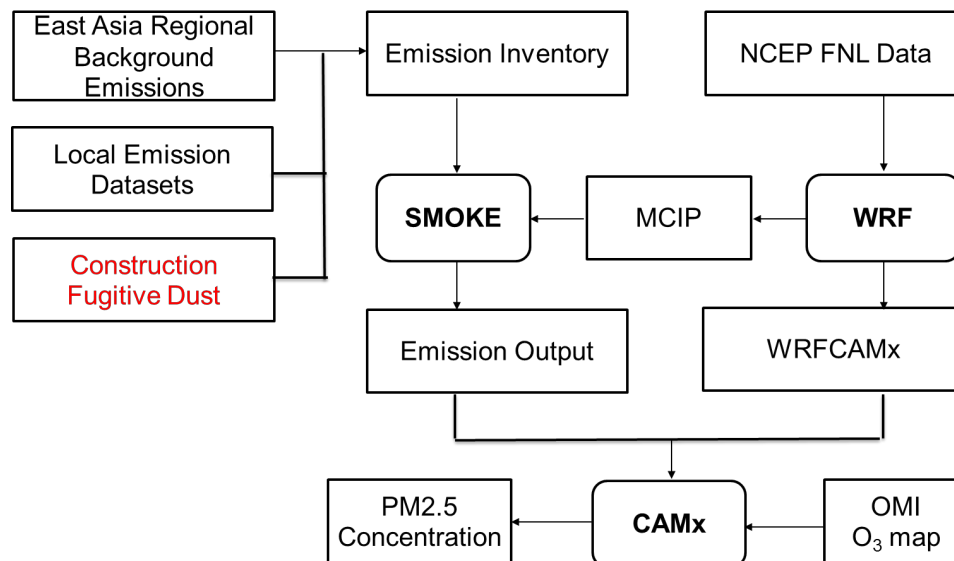
Figure 1. The framework of the WRF-SMOKE-CAMx model system in Xi'an. OMI O₃ map prepares ozone column input files for CAMx to improve the photolysis rate calculation. The CAMx forecasted the air pollutant for the next 48 hours.

2.1 Meteorological fields

85  For the WRF model configuration, we chose the rapid radiative transfer model (RRTM; Mlawer et al., 1997) and the Dudhia for longwave and shortwave radiation options (Dudhia, 1989), WSM3 cloud microphysics (Hong et al., 2004), the YSU scheme (Hong et al., 2006), the Kain–Fritsch (new Eta) cloud parameterization (Kain, 2004), and 5-layer thermal diffusion scheme (Dudhia, 1996). The meteorological initial and boundary conditions were derived from the National Centers for Environmental Prediction (NCEP) global final analysis data (FNL), with spatial resolution of $1° \times 1°$ and temporal resolution of 6-h. The

90 simulation was performed for the period of November 20, 2016 to January 20, 2017.

  The simulation effect of daily average temperature (T2) and relatively humidity (RH2) simulated by WRF model in domain 3 were primarily validated by the observation data at 7 monitoring stations in Xi'an, which the station map was shown in Fig.2. Some statistical parameters of Appendix A were used to evaluate the model performance and shown in Table 1, and the time series was shown in Fig 3. The ME, R and RMSE of daily average T2 are 1.37℃, 0.80, 1.65℃, respectively, and the simulation

95 shows cooling bias of -0.95℃. The ME and RMSE of daily average RH2 are 6.77% and 8.30%. The correlation coefficient of the relatively humidity is 0.71, which is reasonable. RH2 was slightly overestimated as the MB is 6.22%.

  In previous studies, Yang et al. (2019) used WRF to drive CMAQ model for winter air quality in Xi'an, and the model evaluations for winter in 2016 showed that the MB, ME, R and RMSE of T2 were -2.83℃, 2.83℃, 0.89, 3.29℃, respectively. And the MB, ME, R and RMSE of RH2 were 9.59%, 10.63%, 0.71, 13.43%, respectively. Wu et al. (2010) used the fifth-

100 generation NCAR/Penn State Mesoscale Model (MM5) as meteorological driver for the Nested Air Quality Prediction Modeling System (NAQPMS), and the statistical results showed that the MB and R of T2 were 2.1℃ and 0.84 and those of RH2 were -15.8% and 0.65. Under the same model configuration on WRF model and the same verified sites, Yang et al. (2020) compared the simulated and observed wind speed at a 10 m altitude (W10) in Xi'an station from 20 November 2016 to 20 January 2017. As the results show, the W10 is underestimated. The MB of the W10 is -0.14 m/s. The R of the W10 is 0.63,

105 which indicates a good agreement between the observations and the model results.

  Compared with previous studies, T2 and RH2 in this study have lower MB, ME, and RMSE. The R of T2 is slightly lower than previous studies, while the R of RH2 is higher. Thus, the meteorological simulation of this study is reasonable.
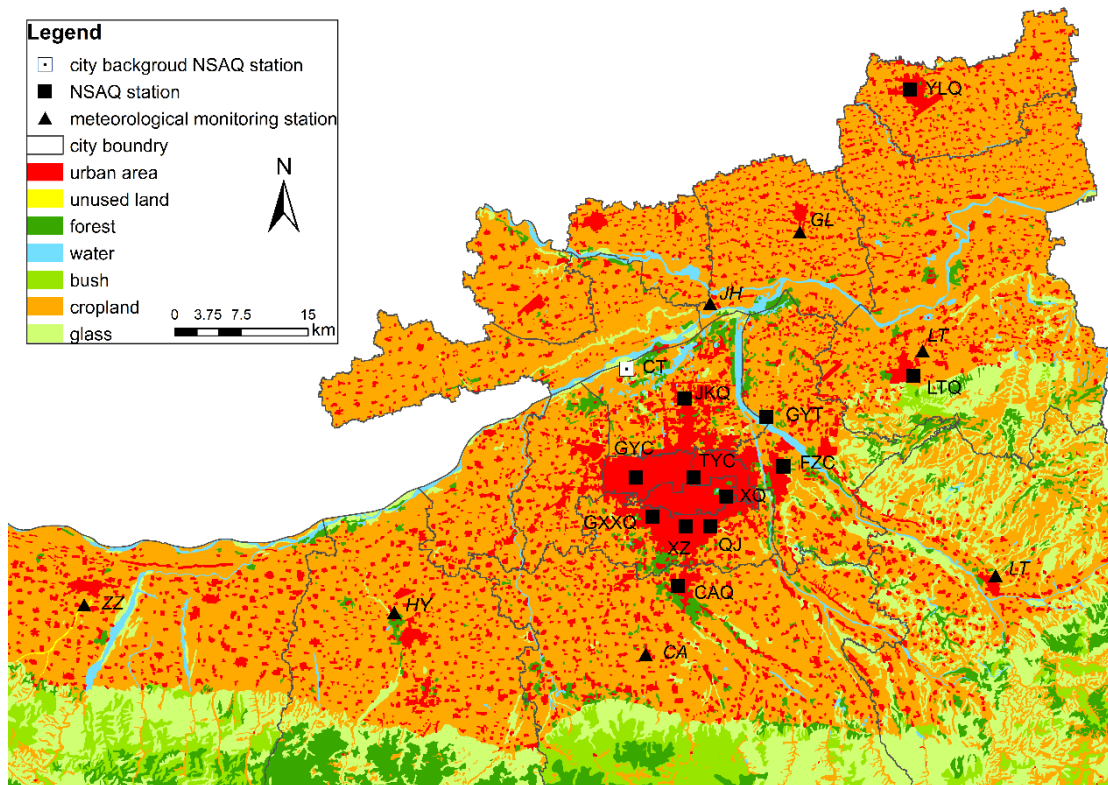
Figure 2. The stations map of the meteorological and air quality monitoring network in Xi'an. The triangles are the meteorological monitoring stations. The square with dot is the city background station and the black squares are the National Standard Air Quality Observation (NSAQ) Stations: Gaoyachang (GYC), Xingqing (XQ), Fangzhicheng (FZC), Xiaozhai (XZ), Tiyuchang (TYC), Gaoxinxiqu (GXXQ), Jingkaiqu (JKQ), Qujiang (QJ), Gaoyuntan (GYT), Changanqu (CAQ), Yanliangqu (YLQ), Lintongqu (LTQ), and Caotan (CT) Station.
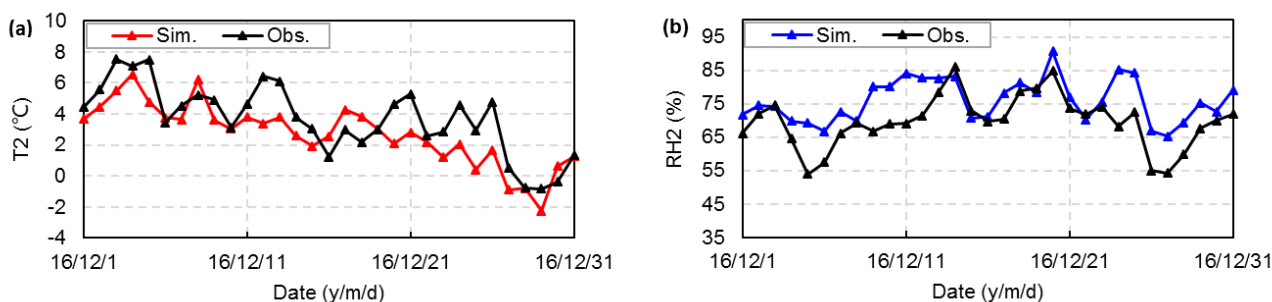
Figure 3. Time series plots of **(a)** daily average simulated and in situ 2m temperature (T2) as well as **(b)** simulated and in situ 2m relatively humidity (RH2) at the Xi'an station.

Table 1. Verification statistics of daily temperature at 2m height (T2), relatively humidity at 2m height (RH2).

Variable	Mean		ME	MB	R	RMSE
	Obs.	Sim.				
T2(℃)	3.68	2.73	1.37	- 0.95	0.80	1.65
RH2(%)	69.65	75.88	6.77	6.22	0.71	8.30

120

2.2 Air quality model descriptions

The CAMx model is a state-of-the-science air quality model, which is developed by the Ramboll Environ (http://www.camx.com). In this study, the PPM advection scheme (Colella and Woodward, 1984) is used for horizontal diffusion, and the K-theory is selected for vertical diffusion. The Regional Acid Deposition Model (RADM-AQ) (Chang et al.,
125 1987) scheme as the aqueous-phase oxidation, ISORROPIA (Nenes et al., 1999) as inorganic aerosol thermodynamic equilibrium, and CB05 (Yarwood et al., 2005) as the gas-phase chemical mechanism, and the Euler-Backward Iterative (EBI) solver with Hertel's solutions (Hertel et al., 1993) is used in the model system. The resistance model for gases (Zhang et al., 2003) and aerosols (Zhang et al., 2001) in dry deposition module, and scavenging model for gases and aerosols (Seinfeld and Pandis, 1998) in wet deposition module is chosen in this study. The CAMx model forecasted the next 48 hours' $PM_{2.5}$
130 concentrations in clean initial simulation testing and will be described more in Sec. 2.3. On the first day, CAMx used the results of the ICBCPREP which can prepare simple, static CAMx initial condition (IC) and boundary condition (BC). On the following days, it used the different initial conditions of the sensitivity experiments.

2.3 Model domain

Three-nest domains were designed for the WRF model (Fig. 4), with a horizontal resolution of 27 km × 27 km (D1), 9 km
135 × 9 km (D2) 3 km × 3 km (D3), respectively. The biggest domain (D1) covered the most parts of China, the second domain (D2) includes Shaanxi Province, Shanxi Province, Henan Province and the inner domain (D3) focused on the 11 cities in Fen-wei Plain, including Xi'an. The CAMx has only one domain and the settings are the same as those in the D3 domain, while focusing on Xi'an as one sensitivity test area for initial conditions and emissions. To reduce the boundary effects, the CAMx model cut down the outermost grid of WRF model and used the variable of the center grid in WRFCAMx module, thus, the
140 CAMx model was three grid cells smaller than the WRF model in D3 domain. The vertical resolution of WRF was 37 layers from the ground to 5 hPa at the top, and 14 layers were extracted by the WRFCAMx module, which can convert the WRF output files into the data format for CAMx model.
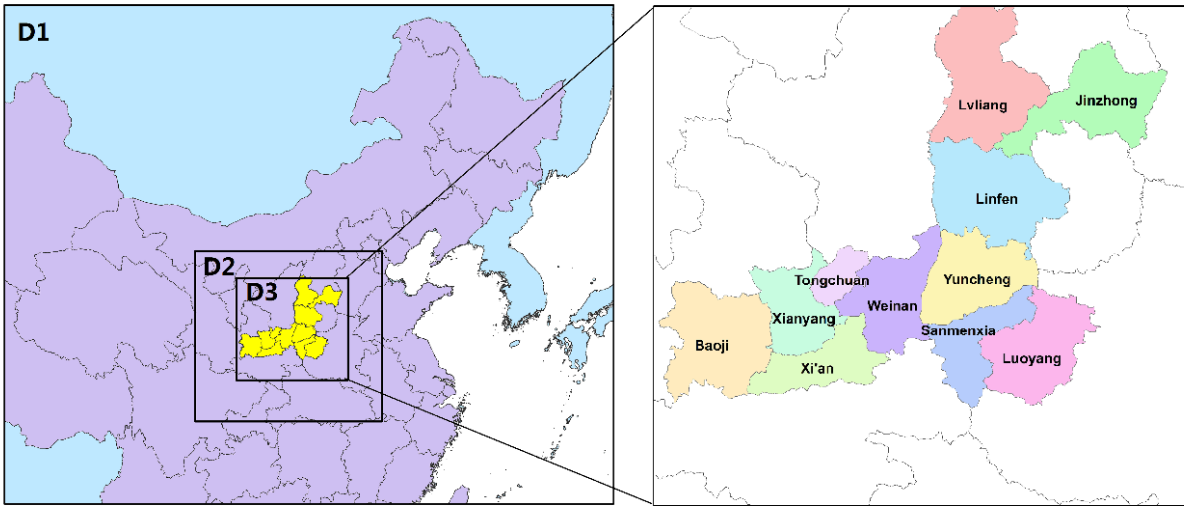
Figure 4. The three-nest model domain with 27-9-3 km horizontal resolution in the WRF-CAMx modelling system. D1 covers
most parts of China, with 148 × 121 grids, and D2 includes Shaanxi, Shanxi and Henan Provinces. The inner domain covers
Fen-wei Plain, including Xi'an.

2.4 Emission Inventory and Processes

The SMOKE version 2.4 (Houyoux and Vukovich, 1999) model was used to improve the Fen-wei emissions, especially
Xi'an local emissions, and provide the gridded emissions for CAMx model in this study. Based on the emission inventories of
previous study (Yang et al., 2019), this study added the emissions quantity of PM$_{2.5}$ from construction fugitive dust in Xi'an
to update the local emission inventories. The emission inventories in this study including:

1. The regional emissions in East Asia and the local emissions in Guanzhong plain were obtained from Wu et al. (2014) and
   Yang et al. (2019). Major industrial emissions had a little adjusted according the annual report in this study. The emission
   inventory in city-level is presented in Table.2.

2. Construction fugitive dust emissions in Xi'an, based on the survey data of construction projects in Fig. 5, were collected in
   the previous study (Xiao et al.,2019), indicated as "local area source". This is new dataset at the county level and update in
   the 2017. The basic data included the location and area of each construction project. Also we replenished the missing
   construction data and correct the error information with Google Earth and other geographic information tools to get more
   accurate location information. According to statistics, there were 1595 construction projects in Xi'an in 2017, with 86.1km^2
   of the total construction area. The construction area in the main urban (Xincheng, Beilin, Lianhu, Yanqiao, Weiyang and
   Yanta) was about 62.2km^2, accounting for 7.5% of the total area in the main urban. The distribution of the construction
   fugitive dust emissions in Xi'an is shown in Fig. 6.

We took the statistics-allocation approach to generate gridded area source emissions, which was to allocate the total emissions to each horizontal model grid according to the related spatial factors. In this study, the Land Scan 2015 Global Population Database (Dobson et al., 2000) was used as a spatial factor of population to allocate the emissions. For the construction fugitive dust emissions, we used the area of each construction project as the weight in the surrogate calculation, allocated the input construction projects data to the target polygons (map of administrative division in Xi'an at the county level) based on weighted spatial overlap of the input data and target polygons. And the spatial results provide to the SMOKE model as spatially allocated factor. The horizontal and vertical allocation of point source emissions were assigned from their longitude-latitude coordinates and the Briggs algorithm (Briggs, 1972; 1984), respectively. While the temporal variation and chemical species allocation were based on profile files in SMOKE model.

As shown in Table 2, the NOx emissions ranged from 352.0 kt yr^{-1} to 758.5 kt yr^{-1} between 2008 in Zhang et al. (2009) to 2017 in this study. For PM$_{10}$ emissions in Shaanxi Province, the emissions also increased from 474.0 kt yr^{-1} to 830.0 kt yr^{-1}. PM$_{10}$ emission in this study are higher than others, because including the construction fugitive dust. Other emission species such as NOx, SO$_2$, NH$_3$, VOCs and CO are little higher in this study than previous studies.

Table 2. Emission of major anthropogenic species in Shaanxi Province (Unit: 10^3 tons yr^{-1}).

		CO	NOx	VOCs	NH$_3$	SO$_2$	PM$_{10}$	PM$_{2.5}$
	point source	1196.0	534.4	1572.7	-	724.7	321.7	257.5
	area source	3272.5	224.1	471.9	294.0	490.2	508.3	244.9
	Xi'an	964.1	177.5	370.5	23.4	155.4	198.6	82.8
This study	Baoji	628.3	65.8	256.9	32.8	131.0	68.4	41.1
	Xianyang	773.9	93.2	584.5	25.9	173.0	88.6	66.8
	Tongchuan	80.6	45.0	32.2	4.4	27.5	60.5	32.3
	Weinan	561.9	140.3	500.9	30.5	224.7	132.6	103.7
	Shaanxi Prov.	4468.5	758.5	2044.6	294.0	1214.8	830.0	502.3
Zhang et al. 2009	Shaanxi Prov.	3528.0	352.0	491.0	-	907.0	474.0	328.0
CCCPSC, 2011	Shaanxi Prov.	-	521.2	-	-	938.7	580.1	-
Yang et al. 2019	Shaanxi Prov.	4369.0	736.9	1994.1	293.2	1193.7	770.4	534.9
Yang et al. 2020	Shaanxi Prov.	3905.8	575.7	1904.3	287.6	802.3	564.0	398.1
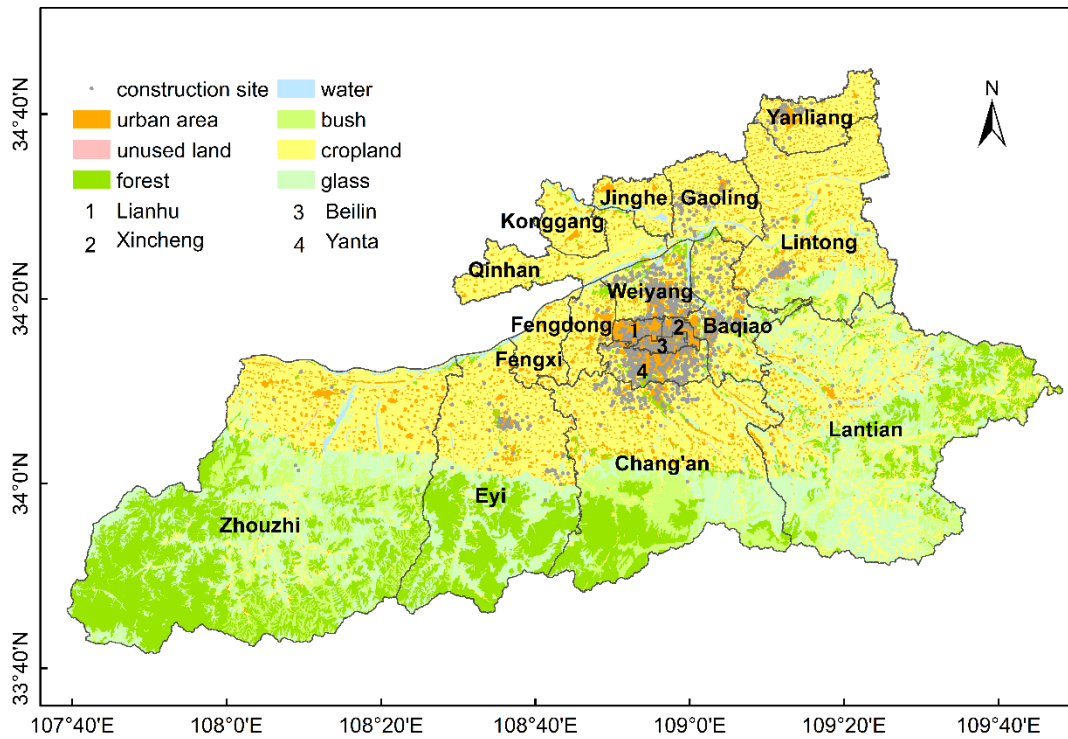
Figure 5. Spatial distribution of construction sites in Xi'an. Gray dots indicate the construction sites. The base map shows the types of land use (Xiao et al., 2019).
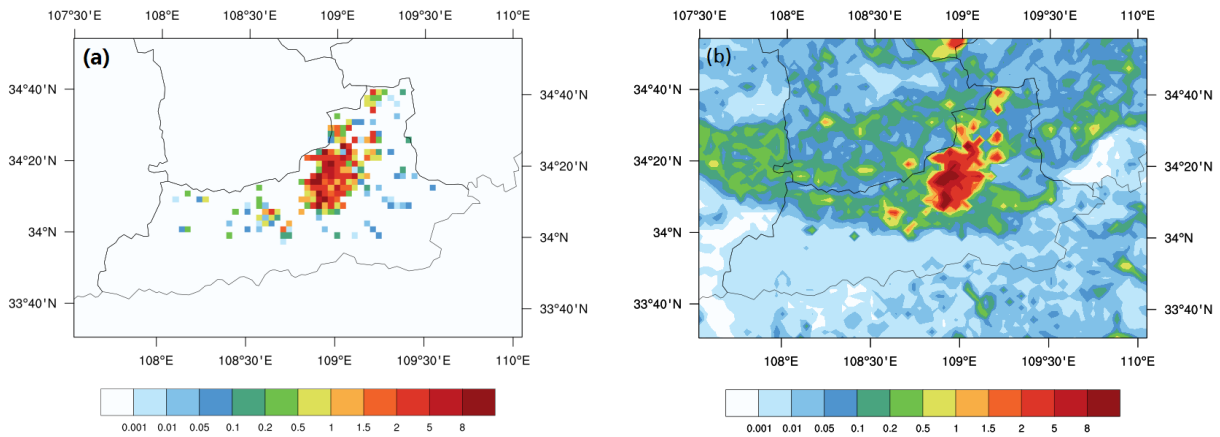
Figure 6. The spatial distribution of PM$_{10}$ emissions in Xi'an and its surrounding area. (a) only construction fugitive dust in Xi'an. (b) all surface PM$_{10}$ emissions in Xi'an. The grid size is 3 km x 3 km. Unit: g/km^2·s

3 Sensitivity experiments design

A set of model sensitivity experiments under different initial conditions and emissions are designed in this study. Three methods were applied for the initial condition tests: using the clean initial condition files as clean initial simulation, using the restart files as restart simulation and the continuous simulation. For the emission tests, we compared the simulation results of the original emission inventory and the updated local emission inventory with construction fugitive dust emissions. The configurations of the simulation sensitivity experiments are shown in Table 3, and the time period for each initial condition experiments are shown in Fig. 7.

3.1 ICON test for using the clean initial condition files

For using the clean initial condition files, icbcprep module used a clean-troposphere vertical profile to generate the initial concentration fields for each day of simulation. The output files of CAMx were initialized at 13:00 UTC. The CAMx model forecasted the next 48 hours' $PM_{2.5}$ concentrations in each cycle simulation. By extracting data from simulated results based on different time periods (0~24h, 6~30h, 12~36h, 18~42h and 24~48h, respectively) shown in Fig. 7 (a), we conducted the sensitivity experiments C00, C06, C12, C18, and C24, and explore the influence of different time periods on the simulation effect of $PM_{2.5}$. For the sensitivity experiment C00, the data of the period for the first 24 h of output file was cut and merged to analyze. And for C06, the first 6 h of data was spin-up time, we cut and merged the data of the period from 19:00 UTC to 18:00 UTC in the second day. C12, C18 and C24 were used the same method to extract and merge data, and the spin-up time of them was the first 12 h, 18 h and 24 h of data, respectively.

3.2 ICON test for using the restart files

The meteorological data of the period 12~36 h was cut to estimate the $PM_{2.5}$ concentrations by restart simulation of CAMx model. For using the restart files, icbcprep module also used clean initial concentration fields at the beginning of the first-day simulation. And gridded three-dimensional instantaneous concentrations of all species on all grids were written at the end of the simulation to allow for a model restart. Then ICON used the 24-h forecast results from the day before as the initial conditions for the following days shown in Fig. 7 (b). The first day of the simulation starts at 12:00 UTC, and the following days starts at 00:00 UTC. In order to explore how long is the spin-up time can eliminate the error caused by the initial value, the sensitivity experiments R1120 and R1124 were set according to the time of the first day for the model simulation, which began on November 20th, 2016 and November 24th, 2016, respectively.

3.3 ICON test for continuous simulation

For the continuous simulation, sensitivity experiments CT12 and CT24 were set according to the start time of the intercepted time periods, which were started at 00:00UTC and 12:00UTC, respectively, shown in Fig. 7 (c). For CT12, the meteorological data of the period 12~36 h was cut and merged to one file. The period 24~48 h was cut and merged for CT24. Also we built

the continuous emission files by SMOKE model. During the simulation, there was no interruption and finally generated a long-term sequence simulation result for each start time.

3.4 Emission test for different emission inventories

Based on the initial condition tests, we selected the best method to do the emission sensitivity experiments. For the emission
220 tests, we compared the simulation results of the original emission inventory (sensitivity experiments Enc) and the updated local emission inventory with the construction fugitive dust emissions (sensitivity experiments Ec).

Table 3. The simulation experiment configurations. C00-C24, R1120, R1124, CT12 and CT24 were used to investigate the impact of simulation methods, start time and extracted time period. The impact of different emission inventory was investigated
225 by Ec and Enc. Method C, R, CT presented for the methods of the clean initial condition simulation, restart simulation and continuous simulation. Emission inventory nc and c presented for the original emission inventory and the updated local emission inventory with the construction fugitive dust emissions, respectively.

Experiment	Method	Emission inventory	Start time and extracted time period
C00	C	c	2016/11/26 0-24th hour
C06	C	c	2016/11/26 6-30th hour
C12	C	c	2016/11/26 12-36th hour
C18	C	c	2016/11/26 18-42th hour
C24	C	c	2016/11/26 24-48th hour
R1120	R	c	2016/11/20 12-36th hour
R1124	R	c	2016/11/24 12-36th hour
CT12	CT	c	2016/11/26 12-36th hour
CT24/Ec	CT	c	2016/11/26 24-48th hour
CT24/Enc	CT	nc	2016/11/26 24-48th hour
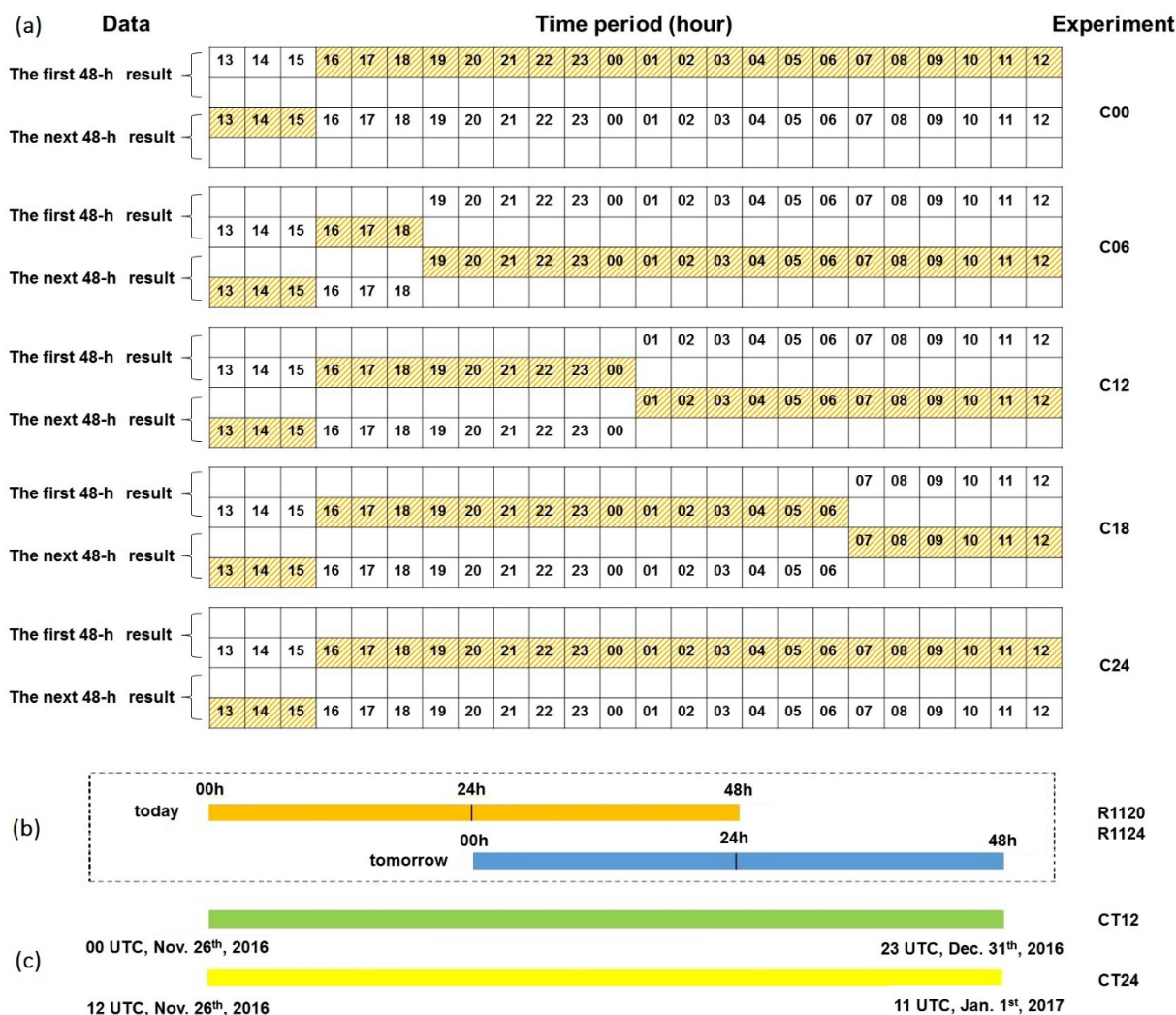
Figure 7. The time period for each initial condition experiments. **(a)** shows the time period for Clean initial condition (mark C) experiments. The first hour results in the output files of CAMx were at 13:00 UTC every day, and the CAMx model forecasted the next 48 hours' PM$_{2.5}$ concentrations in each cycle simulation. The sensitivity experiments C00, C06, C12, C18, and C24 extract different time periods (0~24h, 6~30h, 12~36h, 18~42h and 24~48h, respectively) in each output file as valid data, represented by the grids with number. Each grid represents an hour and the numbers on the grids indicate the hours of the data. The grids with numbers represents the valid time period for each output file. In order to analyze from 0:00 Beijing time (16:00 UTC) every day, the 24-hour data of a day is cut and merged from 16:00 UTC in the valid time period of each output file. And the shaded grids represent the data for one single day. **(b)** shows the time period for Restart (mark R) experiments. The meteorological data of the period 12~36 h was cut to estimate the PM$_{2.5}$ concentrations by restart simulation.

The first day of the simulation starts at 12:00 UTC, and the following days starts at 00:00 UTC. **(c)** show the time period for ConTinuous simulation (mark CT) experiments. The meteorological data of the period 12~36 h is cut and merged to one file for CT12 and the period 24~48 h was cut and merged for CT24.

4 Results and discussion

In this study, we collected the observations in December 2016, and evaluate the model performance and improvement. The model ability from both the meteorological field and the daily PM$_{2.5}$ simulations in Xi'an is evaluated in this study.

4.1 Model performance of the initial condition tests

There are 13 NSAQ Stations in Xi'an which marked as squares in Fig 2. Nine stations are in urban Xi'an,including GYC, XQ, FZC, XZ, TYC, GXXQ, JKQ, QJ and GYT. Three stations are located in suburban towns, including CAQ, YLQ and LTQ. The CT Station is the city background station, which is in northern urban Xi'an.

4.1.1 Sensitivity experiments for using clean initial condition files

Taylor nomogram (Taylor, 2001; Gates et al., 1999) is used to evaluate the accuracy of simulated PM$_{2.5}$ daily concentrations for NSAQ stations which was for the sensitivity experiments of using the clean initial condition files, shown in Fig 8. There are three statistical parameters to evaluate model accuracy, which are the correlation coefficient (R), normalized standard deviation (NSD), normalized root, and mean square error (NRMSE) in Taylor nomogram (Taylor, 2001; Gates et al., 1999; Chang et al., 2004). The sensitivity experiments C00, C06, C12, C18, and C24 were shown by symbols of different colors. We randomly selected 3 stations in urban Xi'an, 2 stations in county towns and a background station to show the simulation results. And the "AVG" meant the average of 13 NSAQ Stations.

As shown in Fig 8, R is 0.36-0.76 for the sensitivity experiments C00, C06, C12, C18, and C24. C24's R is largest and best over all the NSAQ Stations, and C00's is lowest. The NRMSE, which measures the distance from the marker to the REF in Taylor nomogram, is smallest and best for C24, and longest for C00. For NSD, most NSAQ Stations have similar regularity, that is, the NSD values from C00 to C24 are getting closer to "1". The other statistical parameters are presented in Table 4. From experiments C00 to C24, the absolute mean bias (MB) and the mean error (ME) decrease from 51.07 μg/m^3 to 3.72 μg/m^3 and from 74.09 μg/m^3 to 45.82 μg/m^3, respectively. The absolute normal mean bias (NMB) and the normal mean error (NME) decrease from 29.73% to 2.17% and from 43.12% to 26.67%, respectively. And the index of agreement (IOA) increase from 0.50 to 0.8. In general, the model performance of C24 is better than other sensitivity experiments in clean initial simulation tests.
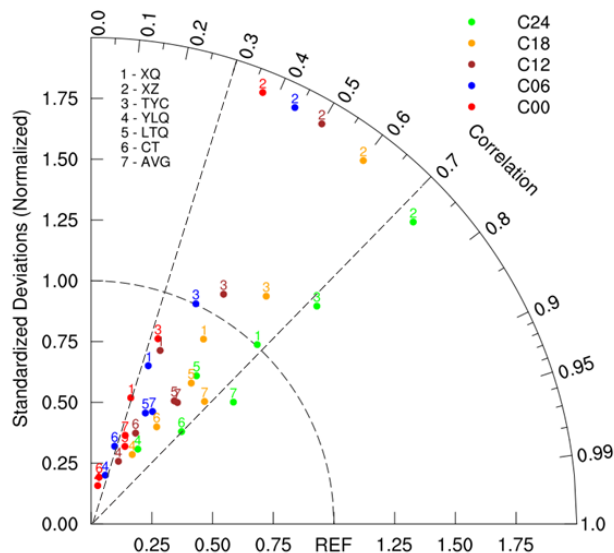
Figure 8. Taylor nomogram for modelled and observed daily averaged PM$_{2.5}$ concentrations for the sensitivity experiment of using the clean initial condition files. The "AVG" meant the average of 13 NSAQ Stations. The sensitivity experiments C00, C06, C12, C18, and C24 were shown by symbols of different colors. REF represents a perfect simulated result according to Chang et al. (2004) for air quality model.

4.1.2 Sensitivity experiments for using restart files

In order to explore the restart simulation, sensitivity experiments R1120 and R1124 were set according to the time of the first day for the model simulation. Starting from 12:00 UTC on November 24th, the PM$_{2.5}$ concentration simulation results of the two sensitive experiments, R1120 and R1124, were shown in Fig 9. At first, the results of the two sensitivity experiments were very different, and then the two lines were gradually fitted until 16:00 UTC on November 25th. After 16:00 UTC on November 25th, the two lines fitted almost completely. Therefore, the spin-up time of 27 hours can eliminate the error brought by the initial field for the PM$_{2.5}$ concentrations in CAMx model.

As shown in Table 4, the model performances of the sensitivity experiments R1120 and R1124 are similar in December, 2016. For the sensitivity experiments R1120 and R1124, the R value between observations and simulations is 0.70. The mean bias (MB) and the mean error (ME) are 4.01 μg/m³ and 49.68 μg/m³, respectively. The normal mean bias (NMB) and the normal mean error (NME) are 2.33% and 28.92%, respectively. The value of root mean square error (RMSE) is 67.28 and the IOA reaches 0.82.
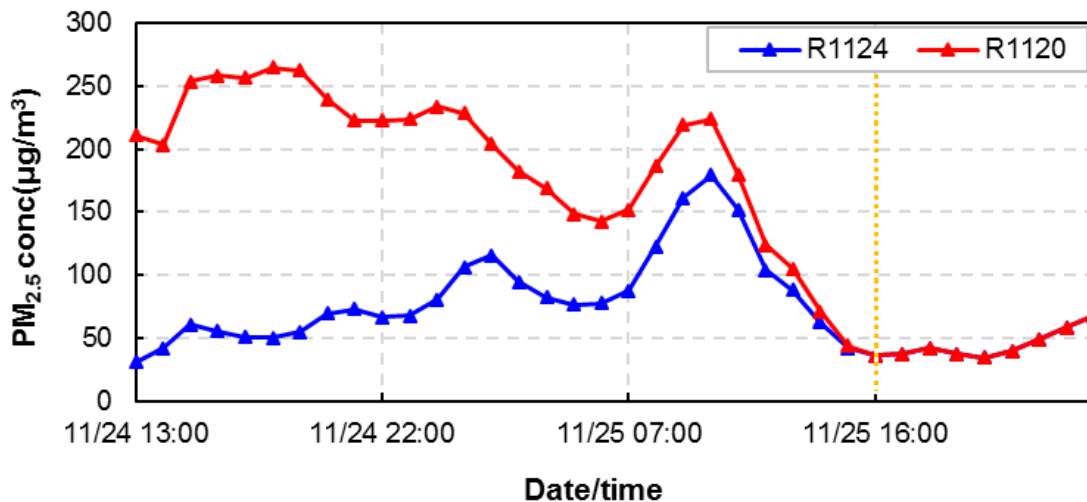
Figure 9. The time series of hourly simulated PM$_{2.5}$ concentrations for using the restart files during a period of the spin-up time. The red and blue lines represent the model sensitivity experiments R1120 and R1124, respectively. The begin day of R1120 for model simulation was November 20th, 2016, and R1124 was November 24th, 2016.

4.1.3 Sensitivity experiments for continuous simulation

As for the continuous simulation, sensitivity experiments CT12 and CT24 were conducted. Although the sensitivity experiments CT12 and R1120 use different methods to generate the initial concentration fields, the start time of the intercepted time periods for the two experiments are the same. PM$_{2.5}$ concentrations of CT12 and R1120 are presented in Fig 10. As shown in Fig 10, the points lie very close to the perfect line "y=x", which indicates that the simulation results of CT12 and R1120 were nearly identical.

The model starting time of sensitivity experiments CT12 and CT24 are November 26th 00:00UTC and November 26th 12:00UTC, respectively. The concentration accumulation of CT24 is 12 hours more than that of CT12. As shown in Fig 11 there is an air pollution peak in December 2016, which CT24 matches better than CT12. The statistical parameters of CT12 and CT24 are presented in Table 4. The mean bias (MB) and mean error (ME) of CT24 results are 6.29 µg/m^3 and 42.67 µg/m^3, respectively, a little better than the CT12 results. The root mean square error (RMSE) of CT24 results is 68.21, also slightly better than the CT12 results. From CT12 to CT24, the R and IOA increase from 0.69 to 0.81 and from 0.81 to 0.90, respectively. Thus, the sensitivity experiments CT24 has better model performance than CT12.
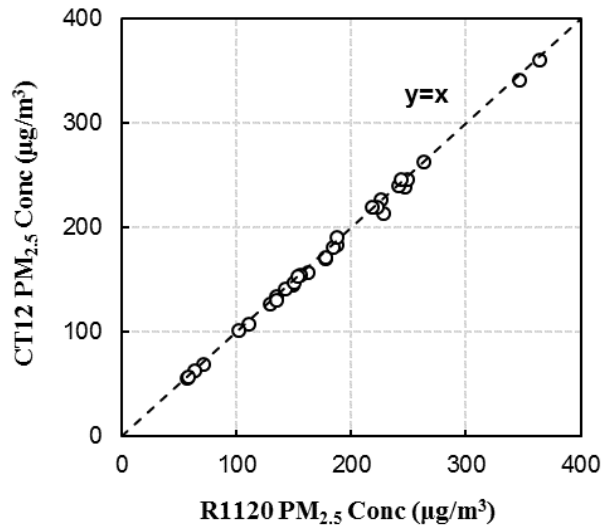
300

Figure 10. Scatter diagram of the R1120 and CT12 experiments of PM2.5 concentrations. Line "y=x" represents the simulated of R1120 is the same to CT12.
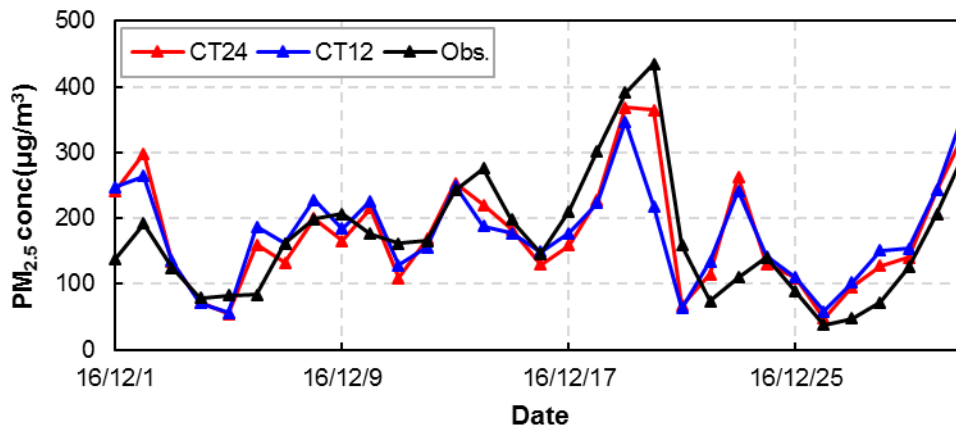
Figure 11. The time series of daily PM2.5 concentrations for continuous simulation in Xi'an. The black line represents
305   observations, the blue and red lines show simulated data started at November 26th 00:00UTC and November 26th 12:00UTC, respectively.

4.2 Model performance of emission tests

Taylor nomogram for modelled and observed daily averaged PM2.5 concentrations for all initial condition sensitivity experiments, shown in Fig 13. The red symbols indicate the sensitivity experiment for using the clean initial condition files,

310 the blue symbols represent the sensitivity experiment for using the restart files, and the brown symbols show the sensitivity experiment for continuous simulation. One experiment per symbol. The circles and triangles represent "bias". As shown in Fig 13, R is 0.36 ~ 0.81 in all initial condition sensitivity experiments. R of CT24 is the largest and best in all initial condition sensitivity experiments. The marker of CT24 has the shortest distance to the "REF" than other initial condition sensitivity experiments, which means that the NRMSE is the smallest. The NSD of CT24 is 0.92, which determines the modeled and

315 observed patterns have more consistent amplitude of variation. According to these statistical parameters, the sensitivity experiments CT24 have the best model performance than other initial condition sensitivity experiments.

Based on the initial condition tests, we selected the best method, CT24, to do the emission sensitivity experiments, shown in Fig 12. CT24 is the experiment with construction fugitive dust emissions (sensitivity experiments Ec) and the sensitivity experiments Enc is not. As shown in fig 12, the simulated $PM_{2.5}$ concentrations of Ec play the better model performance than

320 that of Enc in the high concentration range. As the results shows in Fig 13, R of Ec and Enc are 0.81 and 0.85, respectively. The NRMSE for Enc is smaller than Ec shown in the taylor nomogram. However, the NSD of Ec, 0.92, is better than Enc, 0.74. And the bias of Enc is much larger than Ec. The other statistical parameters are presented in Table 4. The ME decreased from 49.18 μg/m³ to 42.67 μg/m³ and the IOA of simulation results with the updated local emissions reached 0.90. Thus, compared to the simulation results based on the original emission inventory, a new simulation results, which were driven by

325 the updated local emissions, showed a much better performance on $PM_{2.5}$ concentrations.
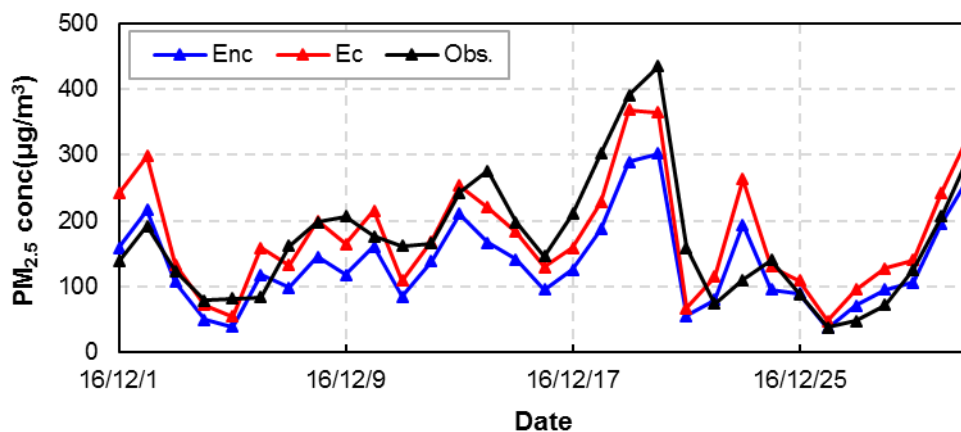
Figure 12. The time series of daily observed and simulated $PM_{2.5}$ concentrations averaged from 13 NSAQ Observation Stations during December 2016 in Xi'an. The black line represents the observations, the blue line represents the simulated by the CAMx model with construction fugitive dust, and the red line represents the simulated values without construction fugitive dust.

330
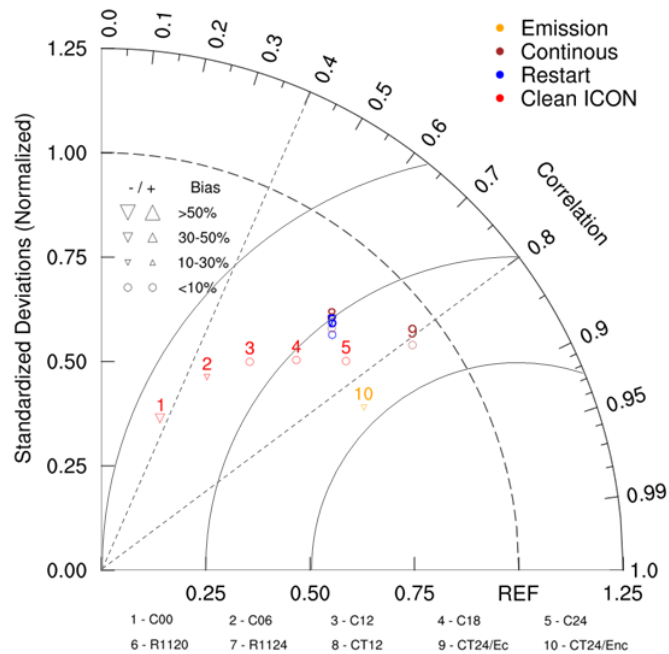
Figure 13. Taylor nomogram for modelled and observed daily PM$_{2.5}$ concentrations for all sensitivity experiments under different initial conditions and emissions. The red symbols indicate the clean initial simulation, the blue symbols represent the restart simulation, the brown symbols show the sensitivity experiment for continuous simulation, and the orange symbols are for emission tests. The triangles and circles signify "Bias". The scale of the triangle's size represents bias value and the direction of the triangle's vertex represents positive or negative.

Table 4. Statistical measures of the modelled daily PM$_{2.5}$ in Xi'an, unit: μg/m.3.

	R	MB(μg/m³)	ME(μg/m³)	NMB%	NME%	RMSE	IOA
C00	0.36	-51.07	74.09	-29.73	43.12	100.72	0.49
C06	0.48	-24.17	60.95	-14.07	35.48	85.50	0.61
C12	0.58	-12.88	53.25	-7.50	30.99	76.64	0.70
C18	0.68	-7.00	48.83	-4.08	28.42	68.85	0.78
C24	0.76	-3.72	45.82	-2.17	26.67	60.12	0.86
R1120	0.70	4.01	49.68	2.33	28.92	67.28	0.82
R1124	0.70	4.01	49.68	2.33	28.92	67.28	0.82
CT12	0.69	6.73	50.20	3.92	29.22	68.21	0.81
CT24/Ec	0.81	6.29	42.67	3.66	24.83	55.29	0.90
CT24/Enc	0.85	-35.16	49.18	-20.47	28.63	61.22	0.86

4.3 Model performance of SO₂ and NO₂

340   The sulfur dioxide (SO₂) and nitrogen dioxide (NO₂) concentrations are the important precursors of SO₄ and NO₃, parts of particulate matter. Daily observed and simulated SO₂ and NO₂ concentrations averaged from 13 NSAQ Stations under the initial restart simulation. Figure 2 shows the time series of daily average SO₂ and NO₂ concentrations averaged from 13 NSAQ Stations under the initial restart simulation, and the statistical results are listed in Table 1. The model has an obvious overestimation of SO₂, with an average bias of 156.31 µg/m³, and the observed SO₂ concentration is only 18% of the simulated

345   value. The main reason is that the implementation of desulfurization projects for important emission sources such as coal-fired power plants in recent years has not been fully considered, which has led to overestimation of SO₂ emissions in the emission inventory. Li et al. (2017b) found that the SO₂ emissions in China have decreased by 75% during the year 2007 to 2016, that is, SO₂ emissions in 2016 were about 25% of 2007. Also the intensity of emissions reduction has uneven spatial distribution. The model performance of NO₂ concentration is better, the IOA reaches 0.82, and the MB is only 3.32µg/m³. There is high

350   consistency of variation trend between the simulated and observed concentrations of SO₂ and NO₂, with R being 0.81 and 0.75, respectively.
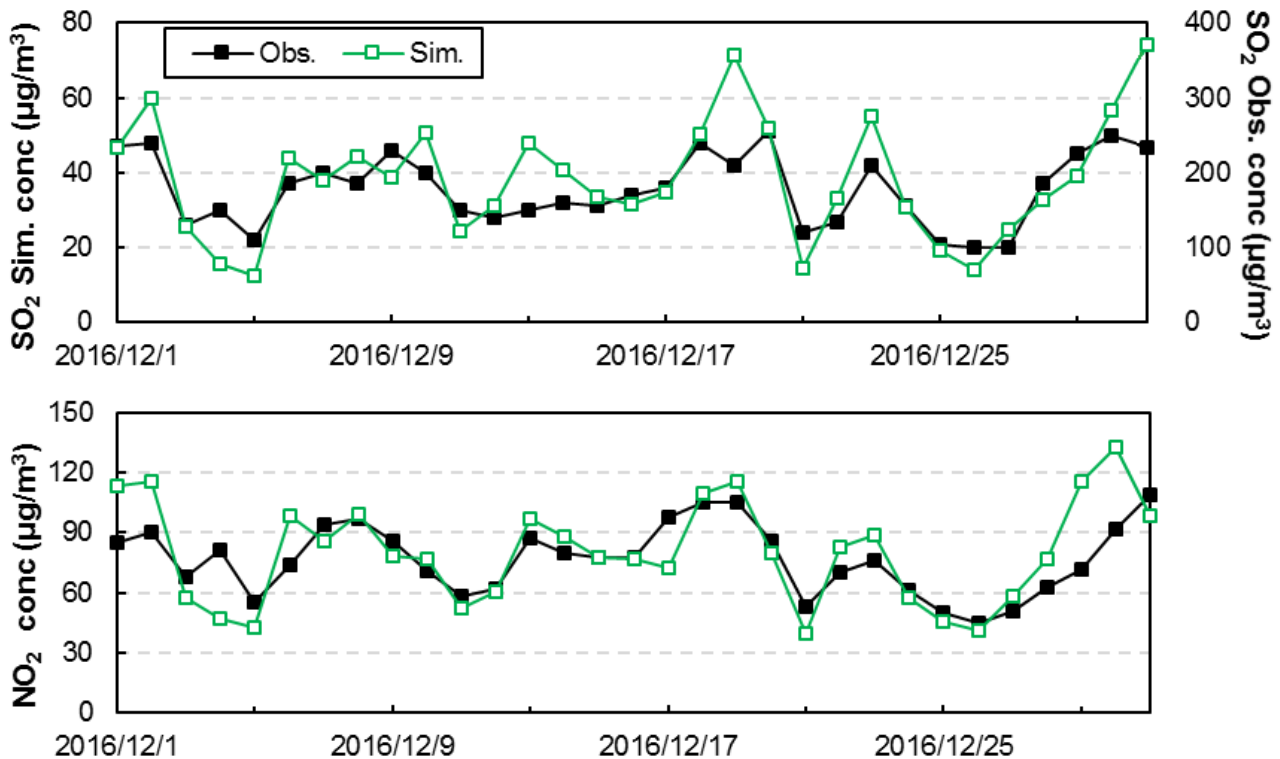
Figure 14. The time series of daily observed and simulated SO₂ (top)and NO₂ (bottom) concentrations averaged from 13 NSAQ Stations during December 2016 in Xi'an. The black and green lines indicate observed and simulated results,

355   respectively.

Table 5. Statistical verification parameters of SO_2 and NO_2 during December 2016 in Xi'an.

Species	Mean($\mu g/m^3$)		R	MB	ME	NMB	NME	RMSE	IOA
	Obs.	Sim.		($\mu g/m^3$)	($\mu g/m^3$)				
SO_2	35.45	191.76	0.81	156.31	156.31	4.41	4.41	171.73	0.11
NO_2	76.77	80.09	0.75	3.32	12.86	0.04	0.17	17.13	0.82

5 Conclusions

The WRF-SMOKE-CAMx model system has been used to simulate the fine particular ($PM_{2.5}$) concentrations in Xi'an in December, 2016. In this study, the emissions of construction fugitive dust in Xi'an were added in the SMOKE to update the local emission inventory. A series of model sensitivity experiments for the initial conditions and emissions are designed to improve the model performance in the megacity, Xi'an.

Three methods were applied for the initial condition tests: using the clean initial condition files as clean initial simulation, using the restart files as restart simulation and continuous simulation. All initial condition sensitivity experiments are driven by the updated emission inventories. The emission tests are based on the initial condition sensitivity experiment which has the best model performance.

Comparing the model performance of $PM_{2.5}$ concentrations in different model sensitivity experiments in Xi'an, we found that the model combining the method of continuous simulation with the updated local emission inventory can nicely improve the model performance. According to statistical parameters, for initial condition tests, the model performance of CT24, C24 and R1120/R1124 are the best. R ranges from 0.36 to 0.81 in all initial condition sensitivity experiments. R of CT24 is the largest and best in all initial condition sensitivity experiments. R of C24 and R1120/R1124 can reach 0.76, 0.70, respectively. The MB of CT24, C24 and R1120/R1124 are lower, which are 6.29 $\mu g/m^3$, -3.72 $\mu g/m^3$ and 4.01 $\mu g/m^3$, respectively. The IOA of CT24, C24 and R1120/R1124 all reach above 0.8, of which CT24 is 0.9. Compared with other methods, the method of using the clean initial condition files has longer simulation time and larger data volume. Therefore, the method of continuous simulation for hindcast, which is to retrieve $PM_{2.5}$ concentrations is suggested. For air quality forecast, we can give priority to the method of restart simulation. Also, for simulating $PM_{2.5}$ concentrations by CAMx model, the simulate needs the spin-up time at least 27 hours. This can improve the simulation effect and reduce the simulation time.

This study updated the emissions inventory, which added construction fugitive dust emissions to the original emissions inventory. Compared to the simulation results based on the original emission inventory, a new simulation results, which were driven by the updated local emissions, showed a much better performance on $PM_{2.5}$ modelling. The absolute MB decreased from 35.16 $\mu g/m^3$ to 6.29 $\mu g/m^3$ and the IOA of simulation results with the updated local emissions reached 0.90. Therefore, the right addition of emissions will also help to improve the effects of simulation and forecasting.

In finally, we recommend the method of continuous simulation for hindcast, which has the best model performance of PM$_{2.5}$ concentrations, and can also reduce the output of IO files to improve computing efficiency. For forecast, the method of restart simulation is suggested, which can reach similar model performance as the continuous simulation. If the restart simulation cannot be used due to the limitation of computing resources and storage space when forecasting PM$_{2.5}$ concentrations, try to extend the spin-up time as much as possible, at least 27 hours according to this work.

Code and data availability

The source codes of the WRF model version 3.9.1.1 used in this study are available online at https://www2.mmm.ucar.edu/wrf/users/download/get_source.html(NCAR, 2020, last access: 4 June 2020). The CAMx version 6.1 code is available at http://www.camx.com/download/default.aspx(ENVIRON, 2020, last access: 4 June 2020), and the SMOKE version 2.4 code is available at https://www.cmascenter.org/smoke/ (CMAS, 2020, last access: 4 June 2020). The global final analysis data (FNL) are from https://rda.ucar.edu/datasets/ds083.2/(NCEP, 2000, last access: 4 June 2020). The dataset related to this manuscript is available online via ZENODO (https://doi.org/10.5281/zenodo.3824676)(Xiao et al., 2020).

Author contribution

Han Xiao did the simulation and prepared the materials. Qizhong Wu designed the WRF-SMOKE-CAMx modelling system for Xi'an, including emission processes. Xiaochun Yang collected the local emission inventory in Shaanxi province and help emission processes. Lanning Wang and Huaqiong Cheng help to prepare the model dataset and figure.

Acknowledgements

The National Key R&D Program of China (2017YFC0209805), the National Natural Science Foundation of China (41305121) and the Beijing Advanced Innovation Program for Land Surface funded this work.

Appendix A

Statistical parameters for the model evaluation:

Mean bias (MB):

$$MB = \frac{\sum(M_i - O_i)}{n} \qquad (A1)$$

Mean error (ME):

$$ME = \frac{\sum|M_i - O_i|}{n} \qquad (A2)$$

Normalized mean bias (NMB):

$$\text{NMB} = \frac{\sum(M_i - O_i)}{\sum O_i} \qquad (A3)$$

410 Normalized mean error (NME):

$$\text{NME} = \frac{\sum|M_i - O_i|}{\sum O_i} \qquad (A4)$$

Root Mean Square Error (RMSE):

$$\text{RMSE} = \left[\frac{1}{n}\sum_{i=1}^{n}(M_i - O_i)^2\right]^{\frac{1}{2}} \qquad (A5)$$

Correlation coefficient (R):

415 $$\text{R} = \frac{\sum_{i=1}^{n}(M_i - \bar{M})(O_i - \bar{O})}{\sqrt{\sum_{i=1}^{n}(M_i - \bar{M})^2 \sum_{i=1}^{N}(O_i - \bar{O})^2}} \qquad (A6)$$

Index of agreement (IOA):

$$\text{IOA} = 1 - \frac{\sum_{i=1}^{n}(M_i - O_i)^2}{\sum_{i=1}^{n}(|M_i - \bar{O}| + |O_i - \bar{O}|)^2} \qquad (A7)$$

Normalized Standard Deviations (NSD):

$$\text{NSD} = \frac{\sqrt{\frac{\sum_{i=1}^{n}(M_i - \bar{M})^2}{n}}}{\sqrt{\frac{\sum_{i=1}^{n}(O_i - \bar{O})^2}{n}}} \qquad (A8)$$

420 In the equations, M_i and O_i represent the simulated value and observation value of a station, respectively. n represents the number of stations. $\bar{M}$ and $\bar{O}$ represent the average value of simulated value and observation value, respectively.

References

Appel, K. W., Napelenok, S. L., Foley, K. M., Pye, H. O. T., Hogrefe, C., Luecken, D. J., Bash, J. O., Roselle, S. J., Pleim, J. E., Foroutan, H., Hutzell, W. T., Pouliot, G. A., Sarwar, G., Fahey, K. M., Gantt, B., Gilliam, R. C., Heath, N. K., Kang, D., Mathur, R.,

425 Schwede, D. B., Spero, T. L., Wong, D. C., and Young, J. O.: Description and evaluation of the Community Multiscale Air Quality (CMAQ) modeling system version 5.1, Geosci. Model Dev., 10, 1703–1732, https://doi.org/10.5194/gmd-10-1703-2017, 2017.

Briggs, G.: Discussions on chimney plumes in neutral and stable surroundings, Atmos. Environ., 6, 507–510, 1972.

Briggs, G.A.: Plume rise and buoyancy effects, Atmospheric Science and Power Production, 327–366, 1984.

430 Cao, G., Zhang, X., Gong, S., An, X., and Wang, Y.: Emission inventories of primary particles and pollutant gases for China, Chinese Sci. Bull., 56, 781–788, https://doi.org/10.1007/s11434-011-4373-7, 2011.

Cao, J.J., Shen, Z.X., Chow, J.C., Watson, J.G., Lee, S.C., Tie, X.X., Ho, K.F., Wang, G.H., and Han, Y.M.: Winter and summer $PM_{2.5}$ chemical compositions in fourteen Chinese cities, J. Air Waste Manage., 62, 1214–1226, https://doi.org/10.1080/10962247.2012.701193, 2012.CCCPSC: The Pollution Source Census Data Set (Statistic),

435   Collected Works about the First China Pollution Source Survey Data (V), Compilation Committee of China Pollution Source Census I, China Environment Science Press, Beijing, 228–245, 2011.

CCCPSC: The Pollution Source Census Data Set (Statistic), Collected Works about the First China Pollution Source Survey Data (V), Compilation Committee of China Pollution Source Census I, China Environment Science Press, Beijing, 228–245, 2011.

440   Chang, J.S., Brost, R.A., Isaksen, I.S.A., Madronich, S., Middleton, P., Stockwell, W.R., and Walcek, C.J.: A three-dimensional eulerian acid deposition model: physical concepts and formulation, J. Geophys. Res.-Atmos., 92, 14681-14700, https://doi.org/10.1029/JD092iD12p14681, 1987.

Chang, J. and Hanna, S.: Air quality model performance evaluation, Meteorology and Atmospheric Physics, 87, 167-196, https://doi.org/10.1007/s00703-003-0070-7, 2004.

445   Chen, H. S., Wang, Z. F., Li, J., Tang, X., Ge, B. Z., Wu, X. L., Wild, O., and Carmichael, G. R.: GNAQPMS-Hg v1.0, a global nested atmospheric mercury transport model: model description, evaluation and application to trans-boundary transport of Chinese anthropogenic emissions, Geosci. Model Dev., 8, 2857–2876, https://doi.org/10.5194/gmd-8-2857-2015, 2015.

CMAS: SMOKE version 2.4, available at: https://www.cmascenter.org/smoke/, last access: 4 June 2020.

450   Colella, P., and Woodward, P.R.: The Piecewise Parabolic Method (PPM) for Gas-dynamical Simulations, J. Comput. Phys., 54, 174-201, https://doi.org/10.1016/0021-9991(84)90143-8, 1984.

Dobson, J.E., Bright, E.A., Coleman, P.R., Durfee, R.C., and Worley, B.A.: Landscan: a global population database for estimating populations at risk, Photogramm. Eng. Rem. S., 66, 849–857, 2000.

Dudhia, J.: Numerical study of convection observed during the winter monsoon experiment using a mesoscale two-dimensional
455   model, J. Atmos. Sci. 46, 3077-3107, https://doi.org/10.1175/1520-0469(1989)046<3077:NSOCOD>2.0.CO;2, 1989.

Dudhia, J.: A multi-layer soil temperature model for MM5, The Sixth PSU/ NCAR Mesoscale Model Users' Workshop, Boulder, Colorado, 1996.

Eder, B., and Yu, S.: A performance evaluation of the 2004 release of Models-3 CMAQ, Atmos. Environ., 40,4811-4824, https://doi.org/10.1016/j.atmosenv.2005.08.045, 2006.

460   ENVIRON: User Guide for Comprehensive Air Quality Model with Extensions Version 6.0, available at: http://www.camx.com/files/camxusersguide_v6-00.pdf, 2013.

ENVIRON: CAMx version 6.1, available at: http://www.camx.com/download/default.aspx, last access: 4 June 2020.

Gates, W., Boyle, J., Covey, C., Dease, C., Doutriaux, C., Drach, R., Fiorino, M., Gleckler, P., Hnilo, J., Marlais, S., Phillips, T., Potter, G., Santer, B., Sperber, K., Taylor, K., and Williams, D.: An overview of the results of the atmospheric model
465   inter-comparison project, B. Am. Meteorol. Soc., 80, 29–55, https://doi.org/10.1175/1520-0477(1999)080<0029:AOOTRO>2.0.CO;2, 1999.

Gilliam, R. C., Hogrefe, C., Godowitch, J. M., Napelenok, S., Mathur, R., and Rao, S. T.: Impact of inherent meteorology uncertainty on air quality model predictions, J. Geophys. Res.-Atmos., 120, 12259–12280, https://doi.org/10.1002/2015JD023674, 2015.

470 Grell, G.A., Peckham, S. E., Schmitz, R., Mckeen, S. A., Frost, G., Skamarock, W. C., and Eder, B.: Fully coupled "online" chemistry within the WRF model, Atmos. Environ., 39, 6957-6975, https://doi.org/10.1016/j.atmosenv.2005.04.027, 2005.

Hertel O., Berkowics, R., Christensen, J. and Hov, Ø.: Test of two numerical schemes for use in atmospheric transport-chemistry models, Atmos. Environ., 27, 2591-2611, https://doi.org/10.1016/0960-1686(93)90032-T, 1993.

Hong, S.Y., Dudhia, J., and Chen, S.H.: A revised approach to ice microphysical processes for the bulk parameterization of
475 clouds and precipitation, Mon. Weather Rev., 132, 103-120. https://doi.org/10.1175/1520-0493(2004)132<0103:ARATIM>2.0.CO;2, 2004.

Hong, S.Y., Noh, Y., and Dudhia, J.: A new vertical diffusion package with an explicit treatment of entrainment processes, Mon. Weather Rev., 134, 2318-2341, https://doi.org/10.1175/MWR3199.1, 2006.

Houyoux, M. R. and Vukovich, J. M.: Updates to the Sparse Matrix Operator Kernel Emissions (SMOKE) modeling system
480 and integration with Models-3, The Emission Inventory: Regional Strategies for the Future, Air Waste Management Association, Raleigh, N. C., 1461, 1999.

Huang, R. J., Zhang, Y., Bozzetti, C., Ho, K. F., Cao, J., Han, Y., Daellenbach, K., Slowik, J., Platt, S., Canonaco, F., Zotter, P., Wolf, R., Pieber, S., Bruns, E., Crippa, M., Ciarelli, G., Piazzalunga, A., Schwikowski, M., Abbaszade, G., and Prevot, A.: High secondary aerosol contribution to particulate pollution during haze events in China, Nature, 514, 218–222,
485 https://doi.org/10.1038/nature13774, 2014.

Kain, J. S.: The Kain–Fritsch convective parameterization: An update, J. Appl. Meteorol., 43, 170–181, https://doi.org/10.1175/1520-0450(2004)043<0170:TKCPAU>2.0.CO;2, 2004.

Kato N, and Akimoto H.: Anthropogenic emission of SO_2 and NOx in Asia: Emission inventories, Atmos. Environ., 26, 2997–3017, https://doi.org/10.1016/0960-1686(92)90291-R, 1992.

490 Li, L., Chen, C. H., Fu, J. S., Huang, C., Streets, D. G., Huang, H. Y., Zhang, G. F., Wang, Y. J., Jang, C. J., Wang, H. L., Chen, Y. R., and Fu, J. M.: Air quality and emissions in the Yangtze River Delta, China, Atmos. Chem. Phys., 11, 1621-1639, https://doi.org/10.5194/acp-11-1621-2011, 2011.

Li, L., Cheng, S. Y., Li, J. B., Lang, J. L., and Chen, D. S.: Application of MM5-CAMx- PSAT modeling approach for investigating emission source contribution to atmospheric SO_2 pollution in Tangshan, Northern China, Math. Probl. Eng.,
495 2013, 1-12, https://doi.org/10.1155/2013/136453, 2013.

Li, X., Zhang, Q., Zhang, Y., Zhang, L., Wang, Y., Zhang, Q., Li, M., Zheng, Y., Geng, G., Wallington, T., Han, W., Shen, W., and He, K.: Attribution of $PM_{2.5}$ exposure in Beijing–Tianjin–Hebei region to emissions: implication to control strategies, Sci. Bull., 62, 957–964, https://doi.org/10.1016/j.scib.2017.06.005, 2017a.

Li C, Mclinden C, Fioletov V, et al.: India Is Overtaking China as the World's Largest Emitter of Anthropogenic Sulfur
500 Dioxide, Scientific Reports, 7(1), 14304, https://doi.org/10.1038/s41598-017-14639-8, 2017b.

Li, X. B., Liu, H. B., Zhang, Z. Y., and Liu, J. J.: Numerical simulation of an extreme haze pollution event over the North China Plain based on initial and boundary condition ensembles, Atmospheric and Oceanic Science Letters, 12, 434-443, https://doi.org/10.1080/16742834.2019.1671136, 2019.

505 Long, X., Li, N., Tie, X., Cao, J., Zhao, S., Huang, R., Zhao, M., Li, G., and Feng, T.: Urban dust in the Guanzhong Basin of China, part I: A regional distribution of dust sources retrieved using satellite data, Sci. Total Environ., 541, https://doi.org/10.1016/j.scitotenv.2015.10.063, 1603-1613, 2016.

Mlawer, E.J., Taubman, S.J., Brown, P.D., Iacono, M.J., and Clough, S.A.: Radiative transfer for inhomogeneous atmospheres: RRTM, a validated correlated-k model for the longwave. J. Geophys. Res. Atmos. 102, 16663-16682,
510 https://doi.org/10.1029/97JD00237, 1997.

NCAR: WRF model, available at: https://www2.mmm.ucar.edu/wrf/users/download/get_source.html, last access: 4 June 2020.

National Centers for Environmental Prediction/National Weather Service/NOAA/U.S. Department of Commerce. 2000, updated daily. NCEP FNL Operational Model Global Tropospheric Analyses, continuing from July 1999. Research Data Archive at the National Center for Atmospheric Research, Computational and Information Systems Laboratory.
515 https://doi.org/10.5065/D6M043C6, last access: 4 June 2020.

Nenes, A., Pandis, S.N., and Pilinis, C.: Continued development and testing of a new thermodynamic aerosol module for urban and regional air quality models, Atmos. Environ., 33, 1553-1560, https://doi.org/10.1016/S1352-2310(98)00352-5, 1999.

Ni, T. R., Han, B., and Bai, Z. P.: Source Apportionment of PM_{10} in Four Cities of Northeastern China, Aerosol Air Qual. Res., 12, 571-582, https://doi.org/10.4209/aaqr.2011.12.0243, 2012.

520 Ohara, T., Akimoto, H., Kurokawa, J., Horii, N., Yamaji, K., Yan, X., and Hayasaka, T.: An Asian emission inventory of anthropogenic emission sources for the period 1980–2020, Atmos. Chem. Phys., 7, 4419–4444, https://doi.org/10.5194/acp-7-4419-2007, 2007.

Panagiotopoulou, A., Charalampidis, P., Fountoukis, C., Pilinis, C., and Pandis, S. N.: Comparison of PMCAMx aerosol optical depth predictions over Europe with AERONET and MODIS measurements, Geosci. Model Dev., 9, 4257–4272,
525 https://doi.org/10.5194/gmd-9-4257-2016, 2016.

Seaman, N. L.: Meteorological modeling for air-quality assessments, Atmos. Environ., 34, 2231–2259, https://doi.org/10.1016/S1352-2310(99)00466-5, 2000.

Seinfeld, J.H., and Pandis, S.N.: Atmospheric Chemistry and Physics, From Air Pollution to Climate Change, John Wiley and Sons, Inc., New York. 1998.

530 Sistla, G., Zhou, N., Hao, W., Ku, J.-Y., Rao, S. T., Bornstein, R., Freedman, F., and Thunis, P.: Effects of uncertainties in meteorological inputs on Urban Airshed Model predictions and ozone control strategies, Atmos. Environ., 30, 2011–2025, https://doi.org/10.1016/1352-2310(95)00268-5, 1996.

Skamarock, W.C., Klemp, J.B., Dudhia, J., Gill, D.O., Barker, D.M., Duda, M.G., Huang, X.Y., Wang, W., and Powers, J.G.: A Description of the Advanced Research WRF Version3 (No. NCAR/TN-475+STR), University Corporation for Atmospheric Research, https://doi.org/10.5065/D68S4MVH. NCAR, 2008.

Streets, D. G., Bond, T. C., Carmichael, G. R., Fernandes, S. D., Fu, Q., He, D., Klimont, Z., Nelson, S. M., Tsai, N. Y., Wang, M. Q., WOO, J. –H., and Yarber K. F.: An inventory of gaseous and primary aerosol emissions in Asia in the year 2000, J. Geophys. Res.-Atmos., 108, 8809-8831, https://doi.org/10.1029/2002JD003093, 2003.

Tang, X., Wang, Z. F., Zhu, J., Gbaguidi, A., and Wu, Q. Z.: Ensemble-Based Surface O3 Forecast over Beijing, Climatic and Environmental Research, 15, 677–684, 2010 (in Chinese).

Taylor, K.: Summarizing multiple aspects of model performance in a single diagram, J. Geophys. Res.-Atmos., 106, 7183–7192, https://doi.org/10.1029/2000JD900719, 2001.

Wang, H., Chen, H., Wu, Q., Lin, J., Chen, X., Xie, X., Wang, R., Tang, X., and Wang, Z.: GNAQPMS v1.1: accelerating the Global Nested Air Quality Prediction Modeling System (GNAQPMS) on Intel Xeon Phi processors, Geosci. Model Dev., 10, 2891–2904, https://doi.org/10.5194/gmd-10-2891-2017, 2017.

Wang, L. T., Zhang, Q., Hao, J. M., and He, K. B.: Anthropogenic CO emission inventory of Mainland China, Acta Scientiae Circumstantiae, 25, 1580–1585, https://doi.org/10.13671/j.hjkxxb.2005.12.002, 2005 (in Chinese).

Wang, P., Cao, J. J., Shen, Z., Han, Y., Lee, S. C., Huang, Y., Zhu, C. S., Wang, Q., Xu, H., Huang, R. J.: Spatial and seasonal variations of PM2.5 mass and species during 2010 in Xi'an, China, Sci. Total Environ., 508, 477-487. https://doi.org/10.1016/j.scitotenv.2014.11.007, 2015.

Wang, Z., Xie, F., Wang, X., An, J., and Zhu, J.: Development and application of nested air quality prediction modeling system, Chinese Journal of Atmospheric Science, 30, 778–790, https://doi.org/10.3878/j.issn.1006-9895.2006.05.07, 2006 (in Chinese).

Wu, D., Fung, J. C. H., Yao, T., and Lau, A. K. H.: A study of control policy in the Pearl River Delta region by using the particulate matter source apportionment method, Atmos. Environ., 76, 147-161, https://doi.org/10.1016/j.atmosenv.2012.11.069, 2013.

Wu, Q., Wang, Z., Gbaguidi, A., Tang, X., and Zhou, W.: Numerical study of the effect of traffic restriction on air quality in Beijing, Sola, 6 (Special Edition), 17–20, https://doi.org/10.2151/sola.6A-005, 2010.

Wu, Q. Z., Xu, W. S., Shi, A. J., Li, Y. T., Zhao, X. J., Wang, Z. F., Li, J. X., and Wang, L. N.: Air quality forecast of PM10 in Beijing with community multi-scale air quality modeling (CMAQ) system: emission and improvement, Geosci. Model Dev., 7, 2243–2259, https://doi.org/10.5194/gmd-7-2243-2014, 2014.

Xiao, H., Wu, Q., Yang, X., Wang, L., Cheng, H.: The dataset of the manuscript "Numerical study of the initial condition and emission on simulating PM2.5 concentrations in Comprehensive Air Quality Model with extensions version 6.1 (CAMx v6.1): Taking Xi'an as example", Zenodo, https://doi.org/10.5281/zenodo.3824676, 2020.

565   Xiao, H., Yang, X. C., Wu, Q. Z., Bai, Q. M., Cheng, H. Q., Chen, X. S., Xue, R., Du, M. M., Huang, L., Wang, R. R., and Wang, H.: Estimate emissions of construction fugitive dust in Xi'an, Acta Scientiae Circumstantiae, 39, 222-228, https://doi.org/10.13671/j.hjkxxb.2018.0377, 2019 (in Chinese).

Yang, X., Wu, Q., Zhao, R., Cheng, H., He, H., Ma, Q., Wang, L., and Luo, H.: New method for evaluating winter air quality: PM$_{2.5}$ assessment using Community Multi-Scale Air Quality Modeling (CMAQ) in Xi'an, Atmos. Environ., 211, 18-28,
570   https://doi.org/10.1016/j.atmosenv.2019.04.019, 2019.

Yang, X., Xiao, H., Wu, Q., Wang, L., Guo, Q., Cheng, H., Wang, R., and Tang, Z.: Numerical study of air pollution over a typical basin topography: Source appointment of fine particulate matter during one severe haze in the megacity Xi'an, Sci. Total Environ., 708, 135213, https://doi.org/10.1016/j.scitotenv.2019.135213, 2020.

Yarwood. G., Rao, S., Yocke, M., and Whitten, G. Z.: Updates to the Carbon Bond chemical mechanism: CB05, Final Report
575   prepared for US EPA. available at: http://www.camx.com/publ/pdfs/CB05_Final_Report_120805.pdf, 2005.

Zhang, L., Brook, J. R., and Vet, R.: A revised parameterization for gaseous dry deposition in air-quality models. Atmos. Chem. Phys., 3, 2067–2082, https://dx.doi.org/10.5194/acp-3-2067-2003, 2003.

Zhang, L., Gong, S., Padro, J., Barrie, L.: A size-segregated particle dry deposition scheme for an atmospheric aerosol module, Atmos. Environ., 35, 549-560, https://doi.org/10.1016/S1352-2310(00)00326-5, 2001.

580   Zhang, Q., Streets, D. G., Carmichael, G. R., He, K., Huo, H., Kannari, A., Klimont, Z., Park, I., Reddy, S., Fu, J. S., Chen, D., Duan, L., Lei, Y., Wang, L., and Yao, Z.: Asian emissions in 2006 for the NASA INTEX-B mission, Atmos. Chem. and Phys., 9, 5131–5153, https://doi.org/10.5194/acp-9-5131-2009, 2009.

Zhang, Q., Klimont, Z., Streets, D. Huo, H. and He, H.: An anthropogenic PM emission model for China and emission inventory for the year 2001, Progress in Natural Science, 16, 223–231, 2006 (in Chinese).

585   Zhang, X.Y., Cao, J.J., Li, L.M., Arimoto, R., Cheng, Y., Huebert, B., and Wang, D.: Characterization of atmospheric aerosol over Xi'an in the south margin of the Loess Plateau, China, Atmos. Environ., 36, 4189–4199, https://doi.org/10.1016/S1352-2310(02)00347-3, 2002.

Zhang, Y., Bocquet, M., Mallet, V., Seigneur, C., and Baklanov, A.: Real- Time Air Quality Forecasting, Part I: History, techniques, and current status, Atmos. Environ., 60, 632-655, https://doi.org/10.1016/j.atmosenv.2012.06.031, 2012.

590   Zhang, Y. P., Li, X., Nie, T., Qi, J., Chen, J., and Wu, Q.: Source apportionment of PM$_{2.5}$, pollution in the central six districts of Beijing, China, J. Clean. Prod., 174, 661-669, https://doi.org/10.1016/j.jclepro.2017.10.332, 2018.